Sea water frozen crystalisation impacted by flow and heterogeneous nucleation: PFM-LBM coupled modelling, simulation and experiments

Jiatong Song[a,1], Da Zhang[b,1], Han Yuan[a*], Ji Zhang[a], Peilin Zhou[c], Yan Li[a], Kunwei Wang[a] and Ning Mei[a]

a. Marine Engineering, College of Engineering, Ocean University of China, 238 Songling Road, Laoshan district, Qingdao, 266100, China

b. School of Energy and Power Engineering, Key Laboratory of Ocean Energy Utilization and Energy Conservation of Ministry of Education, Dalian University of Technology, Dalian, 116024, China

c. Department of Naval Architecture and Marine Engineering, University of Strathclyde, Glasgow G4 0LZ, United Kingdom

Corresponding author: Han Yuan

Phone/Fax: +86-532-66781105,

E-mail: hanyuan@ouc.edu.cn

Address: 238 Songling Road, Laoshan district, Qingdao 266100, China

[1] These authors contributed equally.

Abstract

This study presents a novel phase field method (PFM) - lattice Boltzmann method (LBM) coupled model that describes the ice crystal growth in sea water freezing. Sea water frozen crystalisation impacted by flow and heterogeneous nucleation was numerically and experimentally investigated. The PFM-LBM model was established to conduct simulation. A microscope observation experimental system was built to conduct verification. The results show that flow of sea

This is a peer reviewed, accepted author manuscript of the following research article: Song, J., Zhang, D., Yuan, H., Zhang, J., Zhou, P., Li, Y., Wang, K., & Mei, N. (2022). Sea water frozen crystalisation impacted by flow and heterogeneous nucleation: PFM-LBM coupled modeling, simulation and experiments. Desalination, 524, [115484]. https://doi.org/10.1016/j.desal.2021.115484

water effectively promotes the diffusion of discharged salt and the growth of ice crystals, and reduces the probability of dendrite closure. In the directional competitive growth of ice crystals, the salt content trapped in the ice crystals decreased by 17.4% at 0.025 m/s and 21.9% at 0.05 m/s, while the existence of heterogeneous particles resulted in a narrower the brine channel and higher ice crystal growth rate, of which the ice crystal area increased by 10.8% and the trapped salt content in the ice crystals decreased by 14.8%. The study provides both a methodology of numerically simulate sea ice crystallisation which includes the phase change, solute migration, heat transfer and flow, and a feasible controlling approach to improve desalination efficiency of sea water frozen crystallisation.

Keywords: Freeze desalination; Phase field method; LBM; Heterogeneous nucleation

Nomenclature

Symbols

c	Equilibrium concentration, kg kg^{-1}
C_p	Specific heat, J kg^{-1} K^{-1}
D	Diffusion coefficient，m^2 s^{-1}
e	Velocity component
F	Free energy, J
f	Surface free energy density, J m^{-3} mol^{-1}
g	Double-well potential
h	Monotonously changing function
J	Heat flux
K_T	Thermal conductivity, W m^{-1} K^{-1}
L	Latent heat, kJ m^3
M	Phase-field mobility
Q	Heat per unit volume, w m^{-3}
R	Gas constant, J mol^{-1} K^{-1}
r	Vector direction
T	Temperature, K

u	Velocity, m s^{-1}
V_m	Molar volume, m^3 mol
$\dot{V}$	Velocity correction term
W	Height of the double-well potential
Greek Symbols	
α	Direction
δ_x	Space-step, m
δ_t	Time-step, s
ρ	Density, kg m^3
τ	Dimensionless relaxation time, s
ϕ	Phase-field variable
ω	Weight function
Superscripts/Subscripts	
cc	Bulk solid and liquid
eq	Equilibrium
S	Solid
ss	Speed of sound, m s^{-1}
L	Liquid
Acronyms	
PFM	Phase field method
LBM	Lattice Boltzmann method

1 Introduction

Sea water desalination is a key measure to solve the shortage of freshwater resources. Currently, the most widely used sea water desalination methods are membrane-based methods and distillation-based methods [1,2], which require a large amount of energy during freshwater production. Freezing desalination [3] method, by contrast, consumes lower energy because it utilizes the temperature difference between water and salt crystallisation to separate ice from sea water and the latent heat

of melting (334.7kJ/kg at 1 atm) only 1/7 of that of evaporation (2259.4kJ/kg at 1 atm) [4,5]. The freeze desalination methods generally fall into two categories: direct contact freezing and indirect contact freezing. Direct contact freezing may cause the refrigerant contamination of water products and concentrated brine during freeze desalination due to the probability of hydrate formation [6], while indirect contact freezing can avoid this pollution because the sea water and refrigerants are separated in the crystallizer. Common routes of indirect contact freezing method include suspension and layer freeze crystallisation [7]. It is noted that in suspension freeze crystallisation the sea ice and sea water are mixed together, where the adhering brine on ice slurry surface make it difficult to effectively separate the sea water from the sea ice [8]. Experiments conducted in reference [9] show that the minimum salinity of seawater can merely be reduced from 35ppt to approximately 20ppt with suspension freeze crystallisation method. In comparison, in layer freeze crystallisation larger volume of the ice crystals are formed during the gradual growth of the ice layer, which means the adhering brine on ice layer surface can be reduced and the desalination can be more effective.

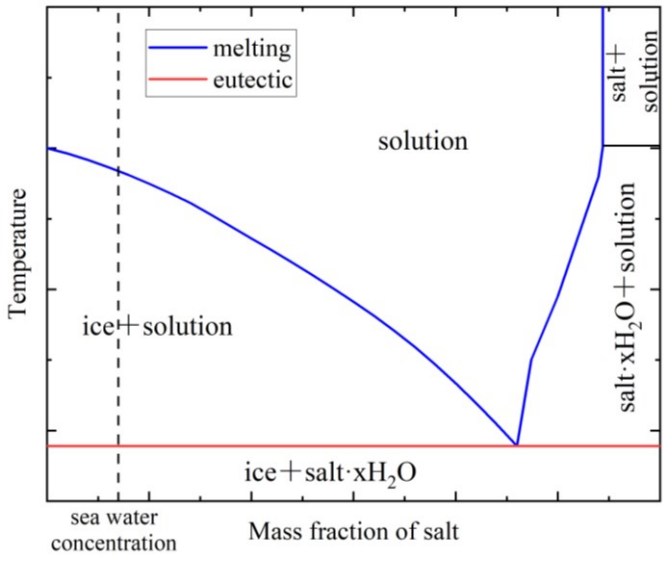

Fig. 1. Salt solution phase diagram

Although freezing desalination have shown a promising prospect, it still faces great difficulties in sea ice purification. The problem lies in sea ice crystallisation mechanism. Fig. 1 shows the salt solution phase diagram. By controlling sea ice crystallisation temperature above the eutectic temperature of water and salt, pure water will crystallise first, so theoretically the water can be separated by freezing desalination method. However, the pockets of concentrated brine are trapped

within ice crystals (named brine pockets) which are hard to remove [10]. This phenomenon results in high concentration in sea ice [11,12], therefore post-treatment technique is needed to purify sea ice. Main purification methods include water washing and centrifugation. However, water washing methods require large amount of fresh water which usually takes up 50% of produced raw ice weight [13], while centrifugation methods need extra power-driven centrifugation and sweeting process [14] to effectively purify the sea ice. These purification techniques are not yet fully effective in terms of cost, large water-handling capacity, and ice net output, and the industrial scale application of freezing desalination remains difficult.

Another option is to conduct pre-treatment technique rather than post-treatment technique and the key point is to inhibit the formation of brine pockets by controlling crystallisation condition. Pre-treatment technique for sea water freeze desalination is in development. Current researches mainly focus on experimental approaches including layer-freezing [15], spray-freezing[16], vertical-freezing [17], radial-freezing [18], suspension crystallisation [19] and ice seeds induced nucleation [13]. These investigations indicate that homogeneous/heterogeneous nucleation mode, crystallisation temperature and heat flux direction all impact the freeze desalination efficiency. These experimental researches have made great contribution in pointing out the way of improving desalination efficiency, nevertheless, the microscopic mechanisms of brine pockets formation and inhibition during the growth of sea ice is still not totally understood. The reason is that the complicated physical processes in freeze desalination such as phase change, solute migration, heat transfer and flow [20] can hardly be thoroughly explained with the macroscopic experiments.

It is worth noting that the phase-field method (PFM) [21] based on the Ginzburg-Landau theory [22] and statistical physics [23] have been developed to solve crystallisation problem [24,25]. PFM employs a concept of diffuse interface instead of traditional sharp interface and utilizes an order parameter to describe the probability of atoms occupying lattice positions within interface. With these two efforts, it no longer needs to precisely describe the complicated two-phase sharp interface of crystals, and this make the crystallisation simulation possible. PFM has shown success in the prediction of metal solidification. But so far, few studies have applied this method to sea water ice crystallisation simulation. In 2013, Berti [26] attempted to rise a phase field model to describe the ice-liquid phase transition in brine channels in sea ice, and the feasibility of PFM in sea ice

simulation was strictly proved for the first time. In 2016, van der Sman [27] present the first model ever that describes the ice freezing phase change in a sugar solution. In 2019, Han [28] attempted to use a Wheeler model to simulate the morphology of ice in binary water-salt. In 2020, our previous work [29] successfully simulated the process of free crystallisation of single crystal nuclei, competitive crystallisation of multi-nuclei, and oriented nuclei in a NaCl-H_2O binary solution based on KKS phase-field model [30]. In 2021, van der Sman [31] established a multiscale simulation model to simulate the directional ice crystal morphology in sugar solutions. However, above proposed models are not entirely satisfactory, because the flow governing equations are not considered in numerical model, making them unable to reveal the impact of fluid convection on sea ice crystallisation. Besides, in these studies sea ice crystal is assumed to experience a homogeneous nucleation process, and the influence of heterogeneous nucleation on sea ice crystal is still not clear.

In this study, we present a novel phase field method (PFM) - lattice Boltzmann method (LBM) coupled model to conduct numerical simulation of sea ice crystallisation. The purpose of this study is to provide a methodology of numerically simulate sea ice crystallisation which includes the phase change, solute migration, heat transfer and flow, as well as a feasible controlling approach to improve desalination efficiency of sea water frozen crystallisation. Both the single sea ice crystallisation which reflects the suspension freeze crystallisation and the directional competitive sea ice crystallisation which reflects the layer freeze crystallisation were investigated. The crystallisation of sea water at different flow rates and the influence of heterogeneous particles on sea ice crystal morphology, solute diffusion, and desalination efficiency were compared, and key parameters such as the tip growth rate and ice crystal area were analysed. A high-definition three-dimensional transmission microscope observation experimental system was built to conduct experimental verification. The impact of sea water flow and heterogeneous nucleation on single/ directional sea ice crystallisation and freeze desalination efficiency were analysed.

2 Mathematical model

2.1 Phase field model coupling with velocity corrective term

The phase-field model is used to couple the phase, solute and temperature fields in the crystallisation process to visualise the crystallisation process and demonstrate the formation process of dendrites directly [32]. The free energy function or entropy function [33] can be combined with

the Ginzburg-Landau theory to derive the phase-field governing equation. Because the expression is not unique, there are multiple phase-field models. This study adopted the KKS phase-field model based on the free energy density function. The KKS phase-field model was revised to construct an ice crystallisation phase-field model suitable for sea ice crystallisation.

2.1.1 Phase field governing equation

Based on the Ginzburg-Landau free energy theory [34], for a closed system with a volume of V, the free energy F can be expressed as:

$$F = \int_V \left[f(\phi, c, e) + \frac{1}{2}\varepsilon^2 (\nabla\phi)^2 + \frac{1}{2}\delta^2 (\nabla c)^2 \right] dV \tag{1}$$

where $f(\phi,c,e)$ is the chemical free energy density[35], ϕ is the phase-field variable defined as a continuous variable between the solid ($\phi = 1$) and liquid ($\phi = 0$) phases, as well as $0 < \phi < 1$ at the solid–liquid interfacial phase; c is the concentration field variable, and ε and δ are the gradient energy coefficient related to the interface anisotropy [35].

$$f(c,\phi,e) = h(\phi) f^S(c_S) + (1 - h(\phi)) f^L(c_L) + Wg(\phi) \tag{2}$$

$$h(\phi) = \phi^3 (10 - 15\phi + 6\phi^2) \tag{3}$$

$$g(\phi) = \phi^2 (1 - \phi)^2 \tag{4}$$

Here, $h(\phi)$ is the monotonously changing function [36] from $h(\phi) = 0$ to $h(\phi) = 1$, $g(\phi)$ is the double-well potential; W is the height of the double-well potential; f^{S} and f^{L} are the chemical potentials of the solid and liquid, respectively; and c_{S} and c_{L} are the equilibrium concentrations of the solid and liquid, respectively.

According to the principle of entropy increase, the free energy gradually tends to decrease until it reaches equilibrium [37]. According to the minimum free energy theory, the Lyapounov function [38] with variational form and the dynamic theory with linear irreversibility can be derived as follows.

The phase-field governing equation of the KKS model [30] is:

$$\frac{\partial \phi}{\partial t} = M[\nabla(\varepsilon^2 \nabla \phi) - f_\phi] \tag{5}$$

where M is the phase-field mobility; f_ϕ is the partial derivative of the free energy density with respect to the phase-field parameter.

Because the phase field is not directly affected by the velocity field, the governing equation of the phase field [30,39] is defined as:

$$\frac{\partial \phi}{\partial t} = M[\varepsilon^2 \nabla^2 \phi - \frac{\partial}{\partial y}(\varepsilon(\theta)\varepsilon'(\theta)\frac{\partial \phi}{\partial x}) + \frac{RT}{V_m} h'(\phi) In \frac{(1-c_L^e)(1-c_S)}{(1-c_S^e)(1-c_L)} - Wg'(\phi)] \tag{6}$$

where c_S and c_L are the equilibrium compositions of solid and liquid, respectively.

The concentration-field equation coupled with the phase field equation[30] is described in the form of the free energy density:

$$\frac{\partial c}{\partial t} = \nabla\left(\frac{D(\varphi)}{f_{cc}}\nabla f_c\right) \tag{7}$$

where $D(\phi)$ is the diffusion coefficient dependent on the phase field, and f_{cc} was added to guarantee a constant diffusion coefficient for both the bulk solid and liquid.

Approximate treatment [40] with dilute solution:

$$D(\phi) = h(\phi) D_S + [1 - h(\phi)] D_L \tag{8}$$

$$\nabla f_c = \nabla \frac{RT}{V_m} In \frac{c_L}{(1-c_L)} \tag{9}$$

$$f_{cc} = \frac{f_{c_L c_L} f_{c_S c_S}}{[1-h(\phi)] f_{c_S c_S} + h(\phi) f_{c_L c_L}} \tag{10}$$

$$f_{c_L c_L} = \frac{RT}{V_m} \frac{1}{c_L(1-c_L)} \tag{11}$$

$$f_{c_S c_S} = \frac{RT}{V_m} \frac{1}{c_S(1-c_L)} \tag{12}$$

The countercurrent behaviour of sea water affects the distribution of salt concentration in sea water, and the influence of flow should be expressed in the governing equation of the concentration field [41]. Assuming that the position of the ice crystals is fixed, the ice crystals generated will not be deformed by the flow pressure difference. The velocity correction term is added to the concentration field control equation to obtain the concentration field control equation coupled with

the velocity field:

$$\frac{\partial c}{\partial t}+\nabla\cdot(\overline{V}c)=\nabla[D(\phi)\nabla c]+\nabla[D(\phi)h^{'}(\phi)(c_L-c_S)\nabla\phi] \tag{13}$$

2.1.2 Temperature field governing equation

It is assumed that the density, specific heat, and thermal conductivity of the solution are constant during the crystallisation process [42]. Considering the release of latent heat of crystallisation, according to the standard heat conduction equation, the following formula is obtained:

$$\frac{\partial Q}{\partial t}+\nabla\cdot J_Q=0 \tag{14}$$

$$J_Q=-K_T\nabla T \tag{15}$$

where Q is the heat per unit volume, J_Q is the heat flux, and K_T is the thermal conductivity.

Considering the change in entropy of the solid–liquid interface, the change in heat per unit volume per unit time [42] can be expressed as:

$$\frac{\partial Q}{\partial t}=C_p\frac{\partial T}{\partial t}-\frac{L}{2}\frac{\partial h(\phi)}{\partial t} \tag{16}$$

where C_p is the specific heat and L is the latent heat.

As the flow of sea water increases the original natural convection of the sea water, the disturbance in the sea water increases, which affects the latent heat released by the ice crystals. Thus, the increase in sea water disturbance promotes the latent heat transfer process. The temperature field control equation of the velocity field coupled with the velocity correction term [30] is expressed as:

$$\frac{\partial T}{\partial t}+\nabla\cdot(\overline{V}T)=D_T\nabla^2T+\frac{1}{2}\frac{L}{C_p}\frac{\partial h(\phi)}{\partial t} \tag{17}$$

2.3 Flow model

The lattice Boltzmann method (LBM) [43] was used to solve the convection during sea ice crystallisation. The two-dimensional, nine-speed model (D2Q9) [44] was selected to conduct simulation. In addition, the fluid flow is considered as incompressible single-phase flow and the flow field is described by a typical single-phase LBM model, which can be found in our previous study [43,44] and other similar study [45,46].

3 Numerical and experimental methods

3.1 Physical model and boundary condition

Ice crystal growth in sea water under both natural convection and force convection conditions, with a domain of 1600 × 1600 meshes simulated, were simulated in this research. Unit mesh size is 0.07μm. To avoid the accumulated latent heat affecting the calculation domain [47], the Neumann temperature boundary conditions instead of zero Neumann boundary conditions are selected. For single sea ice crystals, the location of the circular initial crystal nucleus was set at the centre of the simulation area, with the diameter of 10*dx*. The initial temperature of the simulated area was 285.15 K. In addition, the temperature of sea water flowing into the simulation area was set at 285.15 K. Additionally, when temperature changes from 273K to 285K, the thermal conductivity changed by 2.9%, density changed by 0.072% (seen on Appendix. A), which has no obvious effect on the thermophysical properties. The detailed physical parameters and initial condition are shown in Table 1.

Table. 1. Physical parameters and initial condition in simulation

Physical parameters	Water-NaCl binary solutions
Interface Energy σ, J/m^2	0.0758
Latent Heat L, kJ/kg	335
Equilibrium Constant $k^e=c_L^e / c_S^e$	0.075
Salinity Mass Concentration $\mathcal{C}$, g/kg	0.03
Mesh Number in x axis direction	1600
Mesh Number in y axis direction	1600
Unit Mesh Size, μm	0.07
Time Step, μs	1.72
Mesh Size of Initial Crystal Nucleus Radius	10
Initial Subcooling Degree of Temperature ΔT, K	15
Heat flux σ, J/(m^2·s)	2×10^5

3.2 Numerical simulation methods

The C++ programming language was used to compile the established model, and the main calculation was divided into the following parts:

1 Establishing a sea water physical parameter database.

2 Constructing a basic solution grid matrix.

3 Setting initial conditions, boundary conditions, and phase-field and flow-field parameters.

4 Calculating governing equations for the phase, solute, and temperature fields.

5 Substituting the calculation results into the LBM solving module, and returning to the flow-field distribution after the calculation is complete.

6 Calculating the ice crystal growth parameters.

7 Saving calculation results.

The numerical solution strategy is shown in Fig. 2.

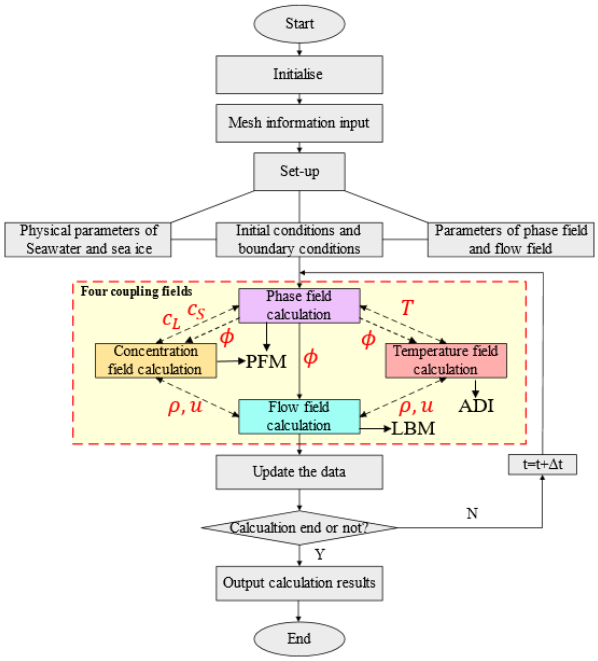

Fig. 2. Numerical solution strategy

The PFM is used to calculate phase field and temperature field, and LBM is applied in solving the flow field. Additionally, the coupled method of PFM and LBM is as following:

Step 1, carry out initialization and boundary setting.

Step 2, calculate phase field and concentration field by PFM, and calculate temperature field by finite difference method (ADI).

Step 3, Exchange information ($C_L, C_S, T, \rho, u, \phi$) of each field.

Step 4, calculate flow field using LBM until the flow domain reaches quasi equilibrium state

($\frac{\sqrt{\sum_x \sum_y [u(x,y,t)-u(x,y,t-1)]^2}}{\sqrt{\sum_x \sum_y [u(x,y,t)]^2}} < 10^{-5}$).

Step 5, loop step 2-4 until the simulation reaches the target condition.

The solid domain is represented in the model as follows: in phase field, ϕ is set as 1; in concentration field, the concentration is set as 0; in flow field, the density and velocity are set as 1 (can be adjusted according to real physical parameter) and 0, respectively. The solid-fluid boundaries in phase field, concentration field and temperature field are solved by PFM, while it is solved by bounce-back boundary of LBM in flow field. In addition, the growing ice crystal is also considered as solid, which is also solved by this method. In this study, the solid particle and ice crystal are all considered as solid domain. In phase field calculation, the order parameter of the two solid domain is set to 1 and the particles are pre-placed in the simulation area during initialization, and its boundary will not change during simulation. Because the order parameter to describe the probability of atoms occupying lattice positions within interface, the interface between ice and solution is can be described by the calculated order parameter, then the solid region of ice crystals is always changing due to the growth of ice crystals.

3.3 Experimental setup and plan

A high-definition three-dimensional transmission microscope observation experimental system was used to verify the simulation results. The schematic diagram is shown in Fig. 3.

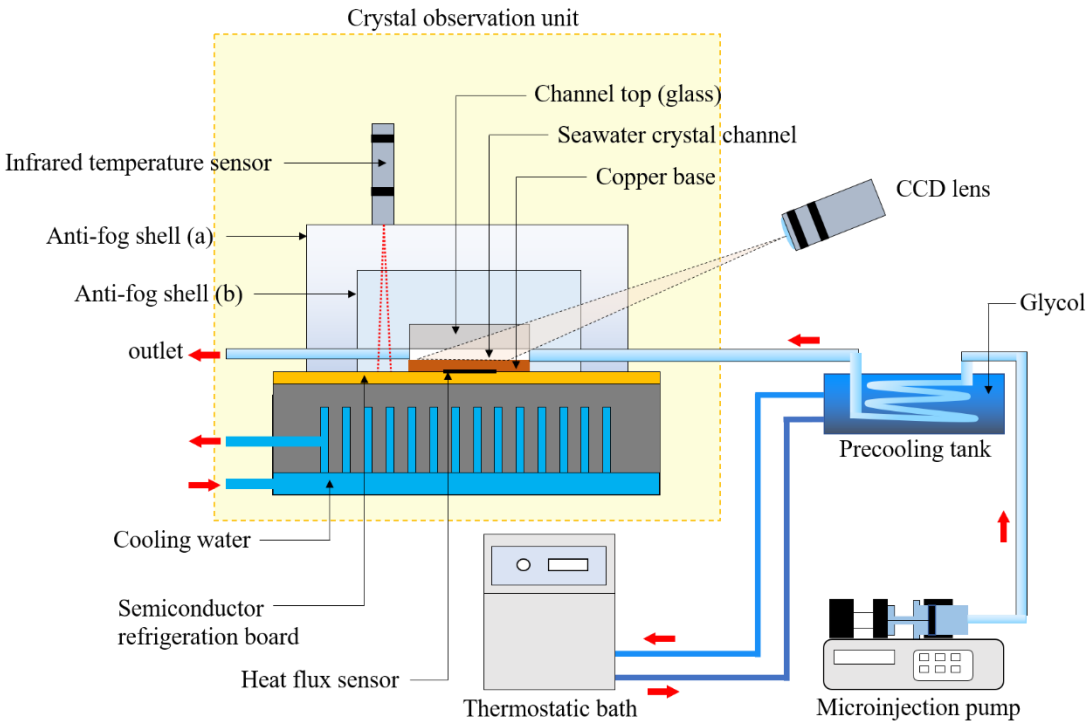

Fig. 3. Schematic diagram of experimental system

The experimental system mainly consists of the crystal observation unit, the transmission microscope and the auxiliary devices. The sea ice crystal channel, in which the sea water get freeze, is sandwiched between top glass and bottom copper base. The copper base is placed on the semiconductor refrigeration board, so that inverse heat flux is applied to the sea ice crystal channel. The heat flux sensor is placed between copper base and semiconductor to measure heat flux during sea ice crystallisation. Besides, the crystal observation unit is covered by two shells, in which the helium is filled to create an anti-fog and adiabatic environment. Both the glass top and copper bottom of the channel wall have been mechanically smoothed to avoid the influence/contamination (i.e. e.g. surface roughness) on the freezing process. In addition, a microinjection pump and a precooling tank are used to preciously control the flowrate and temperature of sea water into the crystal unit, respectively. A high-definition transmission microscope moved by the three-dimensional lens motion controller is used to observe the crystallisation process of sea water. Fig. 4 shows the established experimental system.

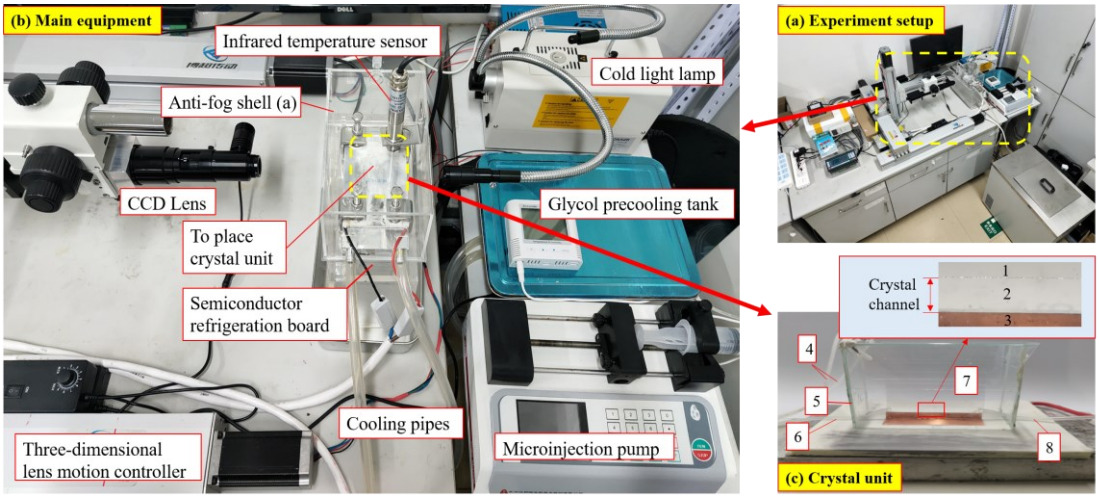

Fig. 4. Diagram of experimental system: 1, Channel top (glass); 2, Seawater; 3, Copper base; 4, Helium inlet/outlet; 5, Anti-fog shell (b); 6, Seawater inlet; 7, Crystal observation unit; 8, Seawater outlet.

In the experimental study, the 31.8-ppt sea water of Qingdao city was used as the crystallisation solution. The experimental supercooling degree was -15 K. Because the single crystal will move along with the enforced flow, experiments were only designed for directional competition growth of sea ice crystals with or without the impact of both flow and heterogeneous particles. Iron particles (diameter at approximately 30 μm) were used as the heterogeneous particles. In order to prevent the influence of accidental error, 3 repeated experiments were carried out in each test. In the experiment, the temperature of the solution flowing into the field of view was -5 °C. The time interval for the control shooting was 3 s, the tip growth rate was calculated at intervals of 0.1 s, and the measurement was started after ice crystals wrapped the foreign particles. The experimental plan is listed in Table 2. In addition, some related studies [48,49] have reported the characteristics of anisotropic morphology of ice crystals, which is a three-dimensional phenomenon. However, according to our experimental observation, if the crystallization occurs in a flat long rectangular channel and the thickness of the ice crystal channel is controlled within 0.01mm, the growth direction of the ice crystal is mainly parallel to the surface of the dendritic ice crystal, rather than the direction of the ice crystal thickness. Therefore, the ice crystal growth characteristics at this time can be characterized by 2D model, which can also be found in our previous research [29].

Table. 2. Experimental plan

Experimental conditions	Flow velocity, m/s	Heterogeneous particles
Test 1	0	✓
Test 2	0	-
Test 3	0.025	✓
Test 4	0.025	-
Test 5	0.05	✓
Test 6	0.05	-

5 Results

In this section, both simulation and experimental results of the impact of flow and heterogeneous particles on the ice crystal growth process are presented. This section mainly focusses on the phenomenon presentation and discussion.

5.1 Impact of flow on sea ice crystals

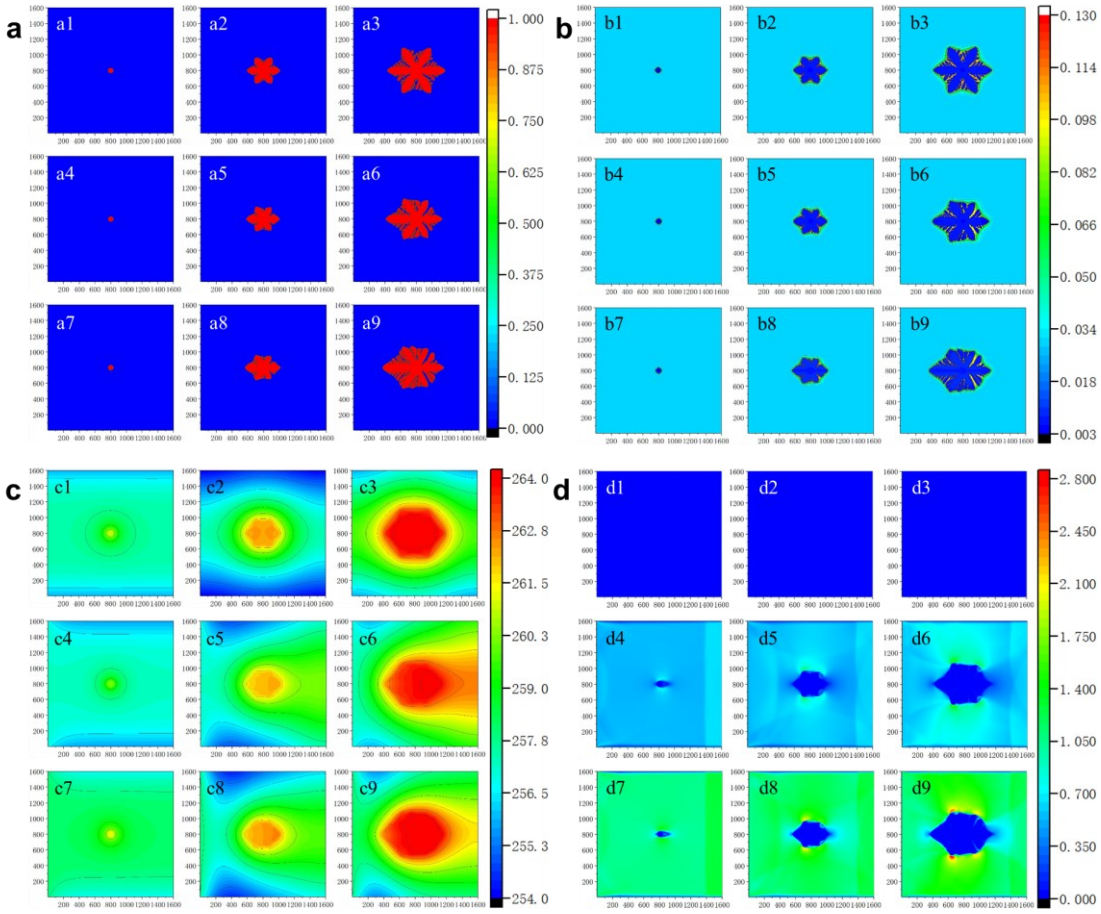

Fig. 5. Simulation results of the phase, concentration, temperature, and velocity fields of the free

growth process of single sea ice crystal at different flow rates, where the initial subcooling degree of temperature is 15K, three velocity conditions are 0 m/s (no sea water flow), 0.5 m/s, and 1 m/s. a: the simulation results of the phase fields; b: the simulation results of the concentration fields; c: the simulation results of the temperature fields, d: the simulation results of the velocity fields;

Fig. 5 shows the phase, concentration, temperature, and velocity fields of the free growth process of single sea ice crystal at different flow rates. In each subfigure, the first, second, and third rows correspond to the simulation results of 0 m/s (no sea water flow), 0.5 m/s, and 1 m/s. Under the influence of ice crystal anisotropy [29], the crystal nucleus preferentially grows in the main axis dendrite in six directions, and then the secondary dendrite grows on the main axis dendrite. The secondary dendrites of different spindles appear in contact with the ice crystal pores [29]. The flow of sea water causes dendrites to grow asymmetrically. The length of the upstream spindle dendrite increased, the secondary dendrites were denser, and the downstream secondary dendrites were less numerous but thicker. The increase in flow velocity increased the asymmetry of ice crystals, the upstream spindle dendrite was longer and thicker, the number of secondary dendrites increased, the number of downstream secondary dendrites decreased, and the dendrite gap increased, which is beneficial for salt discharge. In addition, the related streamline diagrams in Fig 4(d1, d2, d3) are detailed presented in Appendix. A.

The salinity gradient at the tip of the spindle dendrite was greater than that at the tip of the secondary dendrite, which led to a greater growth rate of the spindle dendrite compared with the secondary dendrite. Solute enrichment was observed in the roots of the ice crystals. The sea water flow destroys the distribution of solutes. Upstream solutes accumulated downstream due to flow action [48]. The downstream [49] flow rate was low, and the salt was difficult to diffuse. The concentration gradient upstream of the ice crystal was greater than that downstream, and the growth rates on both sides of the ice crystal differed. A high flow rate promoted the diffusion of solutes. As the flow rate increased, the solute concentration gradient at the tip of the dendrite increased, which was beneficial for the growth of ice crystals.

The thermal diffusion layer at the tip of the main axis of the ice crystal was thinner, forming a larger temperature gradient. The latent heat of the solid phase continued to accumulate, and the latent heat at the root of the ice crystal diffused slowly, resulting in a thicker temperature diffusion

[50] layer at the root of the spindle and a reduced temperature gradient, which inhibited growth of the root. Furthermore, the flow promoted the latent heat transfer. The upstream latent heat was transferred downstream and superimposed with the downstream latent heat, resulting in a higher temperature gradient upstream than downstream. The heat transfer rate increased at high flow rates, and downstream heat accumulation decreased.

The upstream flow velocity of the dendrite was relatively high, while the downstream flow velocity was low, and wake vortex [51] appeared, which promoted solute diffusion and heat transfer. The velocity field became more complicated at high flow rates, and vortices appeared upstream. The high flow rate facilitated the discharge of salt in the dendrite gap, as well as the growth of ice crystals.

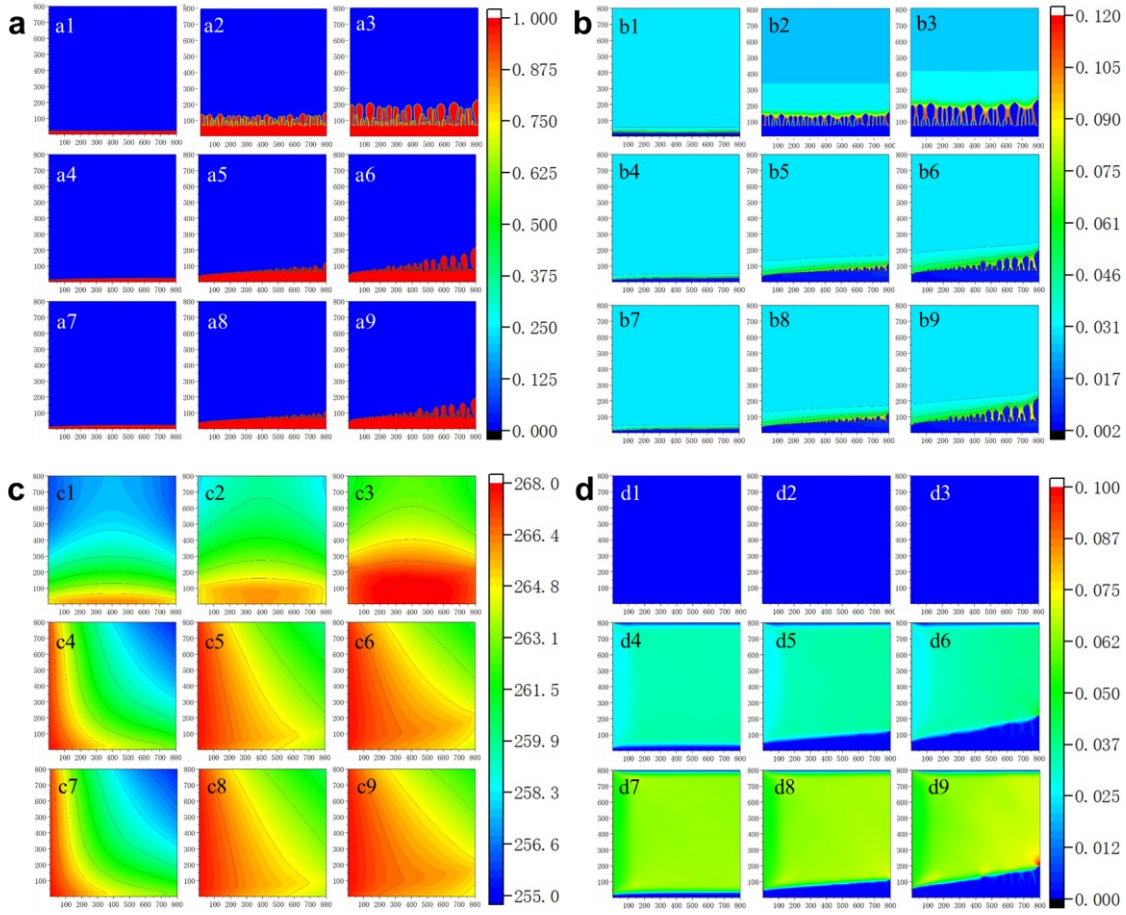

Fig. 6. Simulation results of the phase, concentration, temperature, and velocity fields of the directional competition growth process of sea ice crystals at different flow rates, where the initial subcooling degree of temperature is 15K, three velocity conditions are 0 m/s (no sea water flow), 0.025 m/s, and 0.05 m/s, and the heat flux of bottom boundary is 2×10^5 J/(m^2·s). a: the simulation results of the phase

fields; b: the simulation results of the concentration fields; c: the simulation results of the temperature fields; d: the simulation results of the velocity fields.

Fig. 6 shows the Simulation results of the phase, concentration, temperature, and velocity fields of the directional competition growth process of sea ice crystals at different flow rates. In each subfigure, the first, second, and third rows correspond to the simulation results of 0 m/s (no sea water flow), 0.025 m/s, and 0.05 m/s. It is found that the directional competitive growth of sea water can be divided into two stages. The first stage is uniform upward growth in the form of a plane. In the second stage, differentiated dendrites appear at the top of the plane crystal, demonstrating the competitive growth of multiple dendrites and limited growth of some dendrites. In the case of sea water flow, dendrite differentiation was delayed, and the dendrite was short and sparse. Affected by the temperature of the flowing sea water, the height of the ice crystal on the inlet side of sea water was lower than that on the outlet side of sea water. With an increase in the flow velocity, the dendrite height decreased, the dendrite became finer, the closure trend decreased, and the number of brine pockets decreased. In addition, the related streamline diagrams in Fig 5(d1, d2, d3) are detailed presented in Appendix. A.

The solute field was evenly distributed in the plane crystal stage. During the growth stage of dendrite differentiation, a high concentration of brine pockets discharged from the growth of ice crystals gathered between the dendrites, and the concentration between the dendrites continued to rise, inhibiting the growth of the bottom dendrites, indicating that the dendrite bottom is slender and the top is thick. The flow of sea water promoted the diffusion of solutes, while the concentration of solutes between dendrites was low, and the concentration gradient was small. With a higher flow rate, this effect became more apparent.

The change in the temperature field in the case of no flow was mainly due to the co-action of latent heat and bottom heat flux. The latent heat of crystallisation accumulated at the tip of the ice crystals, and the degree of supercooling decreased, which inhibited the growth of ice crystals. Because the temperature of the flowing sea water was higher than that of the original sea water, the latent heat and heat of the flowing sea water were superimposed, resulting in a temperature peak trend, which greatly reduced the tip supercooling.

The inlet ice crystals of the sea water were thin, the flow area was large, and the ice layer in

the outlet area was thicker, compressing the flow space of the sea water. In addition, the flow velocity of the sea water showed an upward trend. A slower flow rate was exhibited at the tip of the ice crystal, and the solution between the dendrites presented a micro-flow situation. The flow between dendrites became more obvious, and hence promoted the transfer of the solute and the diffusion of heat.

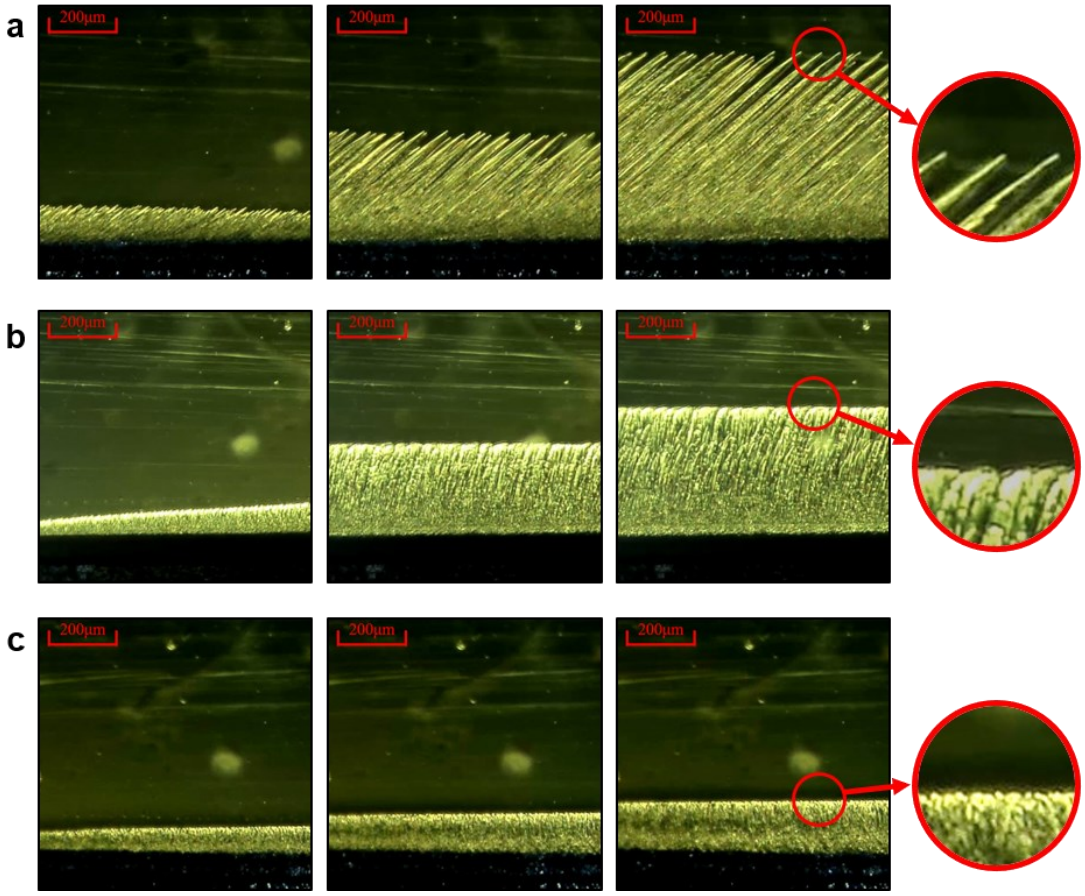

Fig. 7. Experimental verification of the directional competition growth process of sea ice crystals for velocities of a: 0 m/s; b: 0.025 m/s; c: 0.05 m/s, where the supercooling degree is -15 K.

Fig. 7 shows the experimental results of the directional competition growth process of sea ice crystals with the impact of flow. In order to prevent the influence of accidental error, 3 repeated experiments were carried out, and one group was selected and analysed. The results show that at the flow rate of 0 m/s, sea water-oriented crystallised dendrites had finer tips, and the saltwater channels between dendrites were thicker. At the flow rate of 0.025 m/s, the tip of the ice crystals was smooth, and the brine channel narrowed, showing a shrinking trend. The tip of the ice crystal at the flow rate of 0.05 m/s was extremely small, and the brine channel was dense. Meanwhile, the ice crystal growth

rate was fastest at the flow rate of 0 m/s, followed by that at 0.025 m/s, and slowest at 0.05 m/s, which is consistent with the simulation results.

5.2 Impact of heterogeneous particle on sea ice crystals

This part describes the simulations, experiments, and analysis of the influence of heterogeneous particle [52] on the growth of ice crystals. The crystallisation situations of ice single-crystal free growth and directional competition growth were simulated. The program iterated 2,000 steps and recorded the results of the ice crystal growth once.

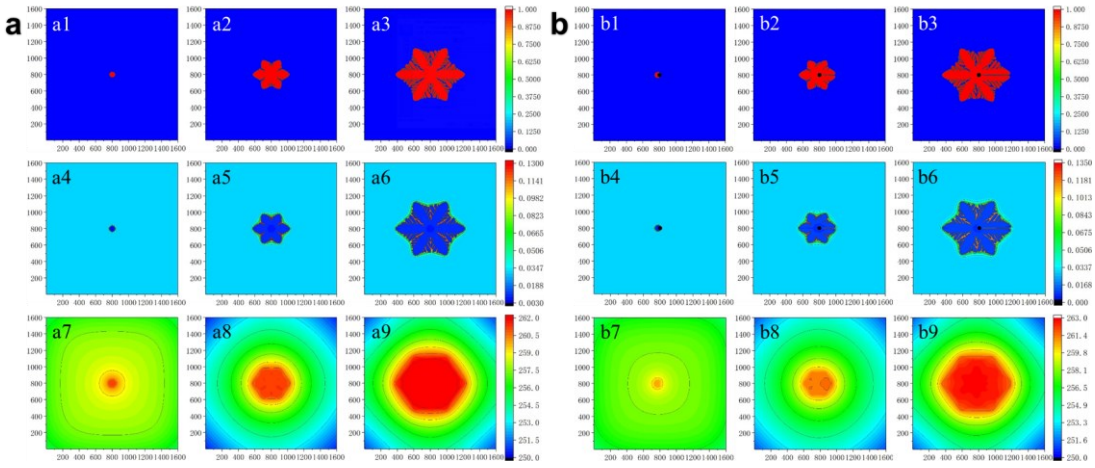

Fig. 8. Comparison of simulation results of ice single-crystal free growth under a: homogeneous nucleation; b: influence of heterogeneous particles, where the initial subcooling degree of temperature is 15K.

The simulation results of single sea ice crystal growth are shown in Fig. 8. In each subfigure, the first, second, and third rows display the simulation results of the phase, concentration, and temperature fields, respectively.

In the homogeneous nucleation condition, the location of the circular initial crystal nucleus was set in the centre of the simulation area with the diameter of 10*dx*. For the influence of heterogeneous particles, the heterogeneous particles were located in the centre of the simulation area with the diameter of 10*dx*, the initial crystal nucleus centre was located on the left side of the heterogeneous particles with the radius of 10*dx*, and the contact angle was 90°.

In the phase field, the phase-field value of the heterogeneous particles was set to -1, the liquid phase part of sea water was 0, the solid phase part was 1, and the solid–liquid interface had a value between 0 and 1. Ice crystals preferentially encapsulated heterogeneous particles during the initial

growth process. Affected by anisotropy, the growth of the ice crystal nuclei was hexagonal, but there was no apparent dendrite differentiation. Because the initial crystal nucleus was located on the left side of the heterogeneous particles, a gap appeared in the right side of the ice crystal when the heterogeneous particles were wrapped. Under heterogeneous nucleation conditions [53], the gap between the main and secondary dendrites of ice crystals was larger than that under homogeneous nucleation. This increase in voids helped the discharge of high-concentration solutions, reduced the number of brine pockets, and reduced the probability of small brine formation.

The concentration field in the presence of heterogeneous particles is basically the same as that in the absence of particles [54]. At the location where the ice crystals are close to the right side of the particle, there was a significant increase in the solute concentration. The salt removal rate was greater than the solute diffusion rate, which led to the accumulation of high-concentration sea water and inhibited the closure of ice crystals.

Moreover, the release of latent heat of crystallisation caused the temperature of the ice crystal centre and the temperature of the heterogeneous particles to rise. The thermal conductivity of the heterogeneous particles is much greater than that of the ice crystals. The supercooling degree of the closed position of the ice crystal is affected by the temperature of the heterogeneous particles and the latent heat of sea ice crystallisation. The supercooling degree was too large, which promoted the growth of the ice crystals to a certain extent.

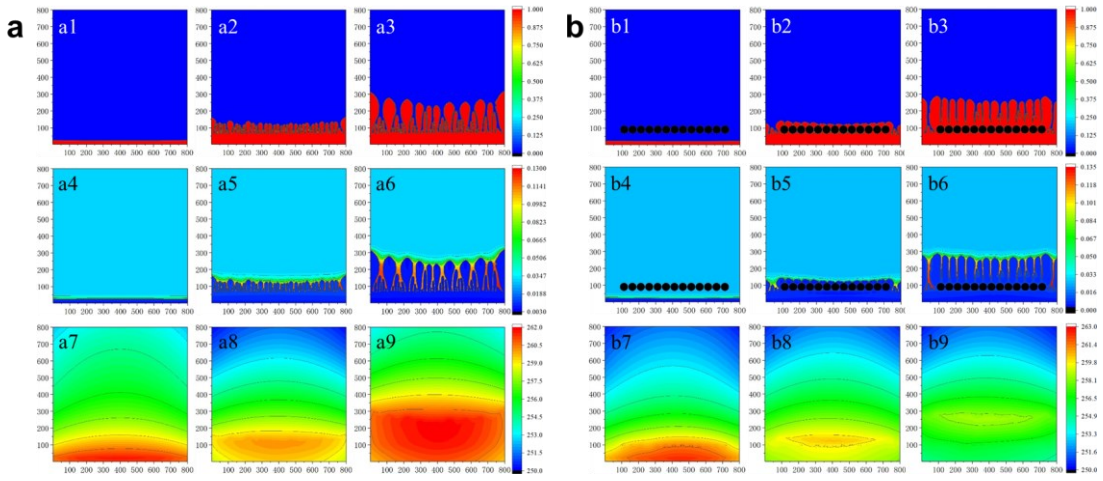

Fig. 9. Comparison of simulation results of the directional competition growth of sea ice crystals under a: homogeneous nucleation; b: influence of heterogeneous particles, where the initial subcooling degree of temperature is 15K, and the heat flux of bottom boundary is 2×10^5 J/(m^2·s).

Fig. 9 shows the simulation results of directional competition sea ice crystal growth. In each subfigure, the first, second, and third rows correspond to the simulation results of the phase, concentration, and temperature fields. It is found that the directional competition growth process of sea ice crystals with and without heterogeneous particles was simulated. The heterogeneous particles were uniformly arranged at the height of 100*dy* with the diameter of 40*dx*, and the centre spacing of different heterogeneous particles was 100*dx*. The initial crystal nucleus was located at the bottom of the simulation area with the length of 800*dx* and height of 5*dx*.

The initial growth process of ice crystals was not affected by the heterogeneous particles and formed flat crystals, similar to homogeneous nucleation. When the ice crystals contacted the heterogeneous particles at 5,000 steps, the growth rate significantly increased. Ice crystals preferentially encapsulated heterogeneous particles, and dendrites began to differentiate after being completely encapsulated, forming saltwater channels. Thus, a relationship exists between heterogeneous particles and ice crystal dendrites. When heterogeneous particles were present, the morphology of ice crystals was more orderly, the dendrites thickened, the brine channels were thinner, the ice crystals grew denser, and the brine pockets at the bottom were clearly reduced.

After the ice crystals contacted the foreign particles, the regions of the foreign particles did not generate high concentrations of brine pockets. There were high-concentration sea water channels on both sides of the heterogeneous particle area. With the growth of ice crystals, high-concentration brine channels formed above the heterogeneous particles, and the concentration was significantly higher than that under homogeneous nucleation conditions. The presence of high-concentration brine in the channel inhibited the growth of ice crystals, hence growth of the secondary dendrites of this part of the ice crystals became difficult, and the probability of forming brine pockets greatly reduced.

The change in the temperature field in the presence of heterogeneous particles is basically consistent with that under homogeneous nucleation, and the highest temperature was located at the tip of the directional-growth ice crystal. Initially, the bottom heat flux dissipated the latent heat of crystallisation, but as the ice crystals gradually grew, the released latent heat gradually accumulated, causing the temperature of the ice crystal tip to first rise and then drop. Because the thermal conductivity of the heterogeneous particles is better than that of ice crystals, the heat transfer is

faster than that of homogeneous nucleation, and the degree of supercooling of the ice crystals around the heterogeneous particles decreased, so that the crystallisation increased and stabilised.

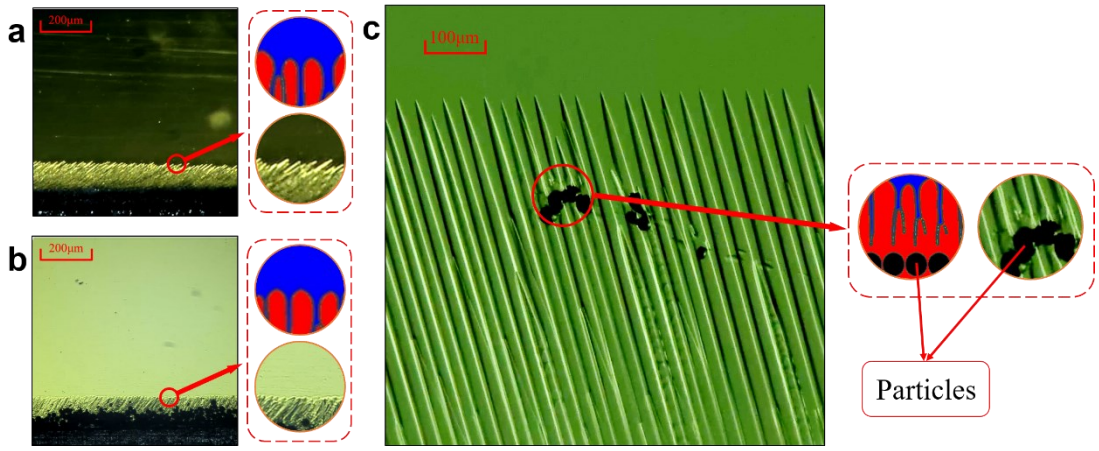

Fig. 10. Comparison of experimental and simulation results of directional competitive growth of ice crystals under different conditions of a: without foreign particles; b: under the influence of heterogeneous particles, located at the bottom of the crystallisation area; c: influence of free heterogeneous particles on the directional growth of ice crystal dendrites.

Fig. 10 shows the comparison of experimental and simulation results of directional competitive growth of ice crystals under different conditions. Enlarged parts show the details of the tips of the ice crystals compared with the simulation results. In order to prevent the influence of accidental error, 3 repeated experiments were carried out. Experimental results of directional competitive growth of ice crystals:

By comparing Fig. 10a and b, the growth state of ice crystals under multi-particle conditions at the bottom is basically the same as that without particles. In the absence of heterogeneous particles, the dendrites appeared slender, the mutual inhibition between the dendrites was serious, and the dominant dendrite growth position was clear. Meanwhile, in the presence of heterogeneous particles at the bottom, the tip of the directional growth of ice crystals was relatively smooth, the tip dendrites were larger, and the dendrites were thicker. The growth heights of different dendrites were basically the same, there was no apparent dendrite inhibition, and the brine channel between the dendrites was narrow, which is basically in line with the results of the simulation.

As can be seen in Fig. 10c, the tip of the ice crystal presented a homogeneous nucleation ice crystal directional competition growth state before contacting the heterogeneous particles. After

contacting the foreign particles, the foreign particles were wrapped, and then the dendrites grew outward. In addition, the dendrites were thicker than before the wrapping. Dendrites exhibited secondary dendrite differentiation as the brine channel narrowed.

6 Discussion

In this section, the influences of flow and heterogeneous particles on the ice crystal growth process are discussed. Each discussion includes two parts: data analysis via simulation and data processing results from the experiment. The main data parameters analysed were the ice crystal area, ice crystal tip growth rate, bottom heat flux change, and dendrite diameter.

6.1 Impact of sea water flow on the growth of ice crystals

The area and growth rate of ice crystals in the simulation were analysed, and the bottom heat flux density and tip growth rate were recorded and processed. The parameters of the ice crystal area and ice crystal tip growth rate were selected for analysis. In the program, the ice crystal area was calculated every 1,000 steps, and the ice crystal tip growth rate was calculated every 100 steps. The speed calculation results were analysed using equation fitting to form a growth speed fitting curve.

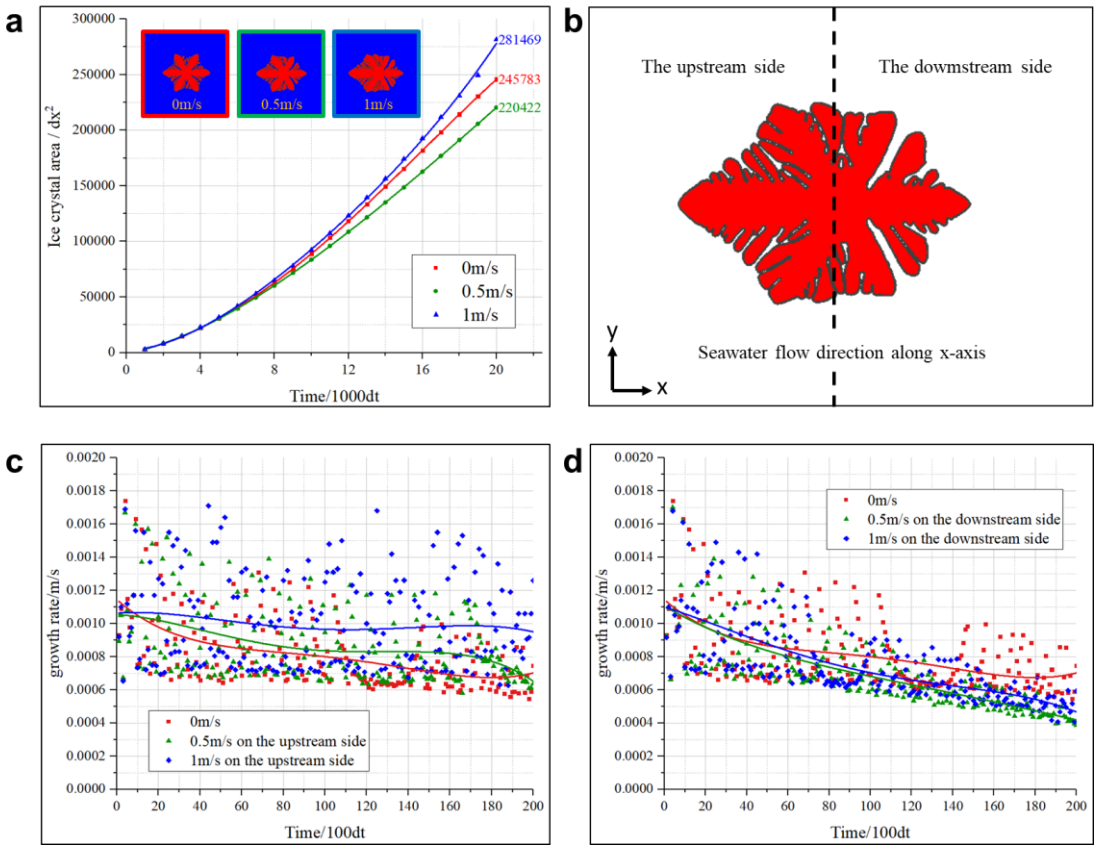

Fig. 11. Analysis of the simulation results of the free growth of ice single-crystals at different flow rates

of a: ice crystal area curve at different flow rates; b: diagram of ice crystal; c: ice crystal upstream growth rate and velocity fitting curve at different flow rates; d: ice crystal downstream growth rate and velocity fitting curve at different flow rates.

Fig. 11 shows the simulation results of the free growth of ice single-crystals at different flow rates. The ice crystal area is based on the grid length (dx), and the unit area is expressed as dx^2. The ice single-crystal area is largest when the flow rate is 1 m/s, followed by that when the sea water is still, and smallest when the flow rate is 0.5 m/s. The difference in the ice crystal area under high and low flow rates is approximately 20%. In the upstream, the ice crystal tip growth rate is largest when the flow velocity is 1 m/s, followed by that when the flow velocity is 0.5 m/s, and smallest when the sea water is still. In the downstream, the ice crystal tip growth rate is the highest when the sea water is stationary, followed by that when the flow velocity is 1 m/s, and smallest when the flow velocity is 0.5 m/s.

From the area of ice single-crystals under static sea water, a low flow rate inhibits the growth of single crystals, while a faster flow rate is beneficial to the growth of the ice single-crystal. The ice crystal area under static sea water is 14.5% less than that at 1 m/s, and 10.3% more than that at 0.5 m/s. Comparing the growth rate of the upstream and downstream sides, the flow of sea water can promote the growth of the upstream ice crystals, while the downstream ice crystal growth is inhibited. The different growth conditions on both sides of the ice crystals also explain the difference in the area of ice crystals at different flow rates.

Upstream, the growth rate of ice crystals increased by 15%-30%, and the effect of flow on ice crystal growth is mainly reflected in promotion of the diffusion of latent heat and solute. The ice crystal tip temperature gradient and solute concentration gradient were large, and the growth rate was stable. Downstream, the growth rate of ice crystal decreases about 10%-20%, and the effect of sea water flow on the diffusion of latent heat and solutes remained, but will transfer the latent heat and solutes from the upstream to the downstream, causing accumulations of the latent heat and solutes, which inhibit the growth of ice crystals. With an increase in the number of iteration steps, the latent heat and solute increased, and the diffusion effect of flow on the latent heat and solute remained stable, resulting in a downward trend in the growth rate of the downstream ice crystal tip.

Upstream, the higher the flow rate, the better the growth of the ice crystals. Whereas,

downstream, owing to the accumulation and diffusion caused by flow, the diffusion effect of lower flow velocity was weaker than the accumulation effect, which inhibits the growth of ice crystals. As the flow rate increased, the diffusion effect gradually strengthened, and the downstream ice crystal growth rate gradually increased. In general, with the increase in the flow velocity, the downstream ice crystal growth rate shows a trend of first declining and then increasing, which also explains the reason for the smallest ice crystal area in the case of 0.5 m/s in the simulation.

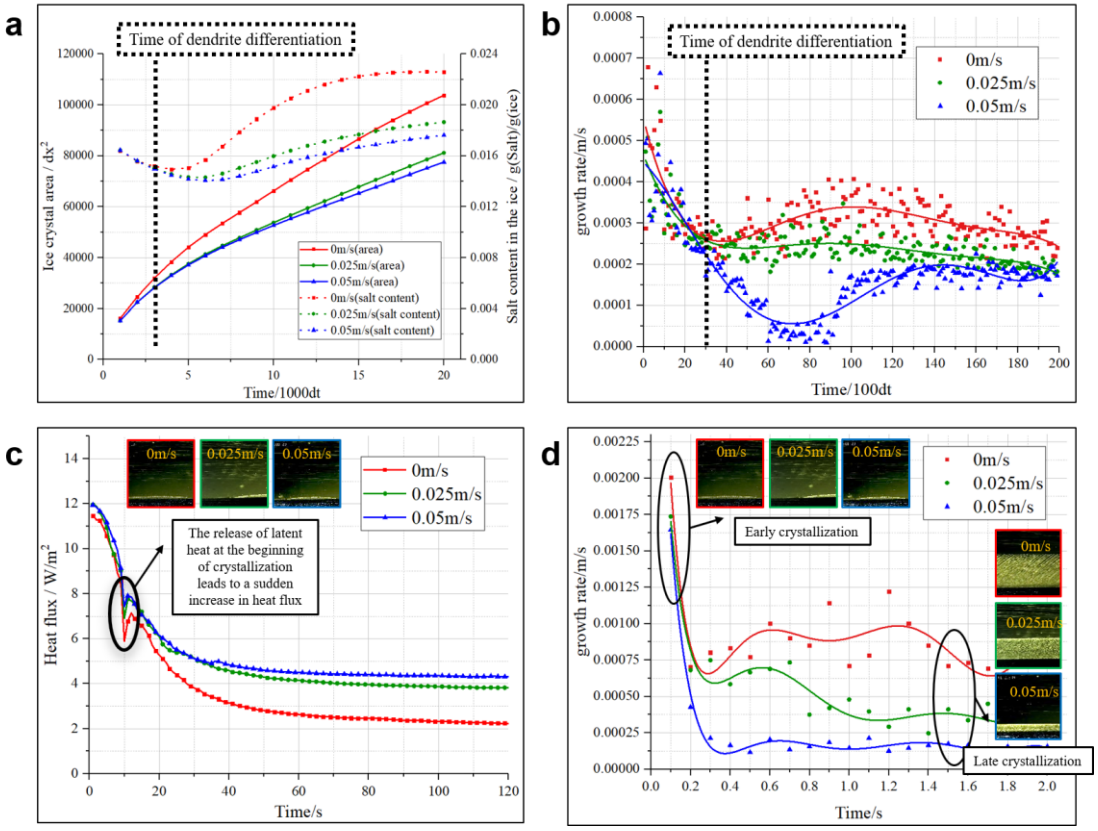

Fig. 12. Simulation and experimental data analyses of the directional competitive growth of ice crystals at different flow rates of a: growth trend of ice crystal area (simulation); b: trend of the tip growth rate (simulation); c: heat flux change at the bottom of the crystallizer (experiment); d: changing trend of the tip growth rate (experiment).

As is shown in Fig. 12a, the ice crystal area is based on the grid length (dx), and the unit area is expressed as dx^2. The area of ice crystals grown by directional competition in stationary sea water is larger than that in the case of sea water flow by approximately 25%. Compared with the ice crystal area under static sea water, the ice crystal area decreased by 21.8% at 0.025 m/s and 25.3% at 0.05 m/s. The heat generated by sea water is a key factor affecting the growth of ice crystals. Regarding the area growth trend, the area of ice crystals grown by directional competition in sea water in the

static state increased much faster than that in the presence of sea water flow. The ice crystal area growth at the flow rate of 0.025 m/s was slightly faster than that at 0.05 m/s, but the overall difference is not significant.

According to Fig. 12b, in the first 3,000 steps of ice crystal growth, the ice crystals grew in the form of planar crystals. The growth rates of the ice crystal tips in the three cases were relatively scattered, and no difference was exhibited. In the initial stage of directional competitive growth of ice crystals, owing to the small amount of crystallisation, the release of latent heat was low, and the flow of sea water had less influence on the ice crystals. In approximately 3,000 steps, the ice crystals began to differentiate. A higher flow rate reduced the supercooling of the ice crystal tip. Although a higher flow rate can remove the latent heat released by the ice crystal and promote the transfer of solute, owing to the influence of the heat of the flowing sea water, the growth of the ice crystal is always inhibited. With an increase in the number of iteration steps, the effect of the bottom heat flux again became apparent, and the growth rate of the ice crystal tip appeared to increase; finally, it reached a dynamic balance with the latent heat of crystallisation and the heat of flowing sea water. In general, under simulated conditions, the growth rate of ice crystals under static conditions is always greater than that in the presence of flow.

Fig. 12c shows the heat flux change during crystallisation. It is found the change in heat flux caused by the temperature difference between the bottom of the crystallizer and the wall of the refrigerating plate was measured during the crystallisation process in the experiments. The initial temperature of sea water was higher than the wall temperature, and the heat flux in the figure shows a downward trend. At 10 s, the sea water began to crystallise, and the latent heat of crystallisation released caused the heat flux density to suddenly rise. As time increased, the temperature difference between the cold wall surface and crystallizer gradually decreased, and the heat flux density decreased slowly. In the case of sea water flow, the value of the crystallisation heat flux caused by the heat generated by the sea water was stable, compared with the case of static sea water. At a higher flow rate, more heat is transferred by the sea water, resulting in differences in the heat flux density at different flow rates.

Fig. 12d shows that under the experimental conditions, owing to the influence of the heat flux on the bottom surface, the ice crystal growth rate under the three flow rates was extremely fast in

the initial stage of ice crystal growth, but the duration was very short. With the increase in time, the growth rates of ice crystals under the three flow rates showed a steady state of fluctuation. The heat from the flowing sea water caused a difference in the growth rate of ice crystals under the three conditions. The growth rate at the flow rate of 0.05 m/s was lowest and the most stable.

6.2 Impact of homogeneous particles on the growth of ice crystals

In this section, the area and growth rate of ice crystals in the simulation were analysed, and the ice crystal dendrite diameter and tip growth rate in the experiment were recorded and processed. The selection of the calculation points was consistent with that in the flow state.

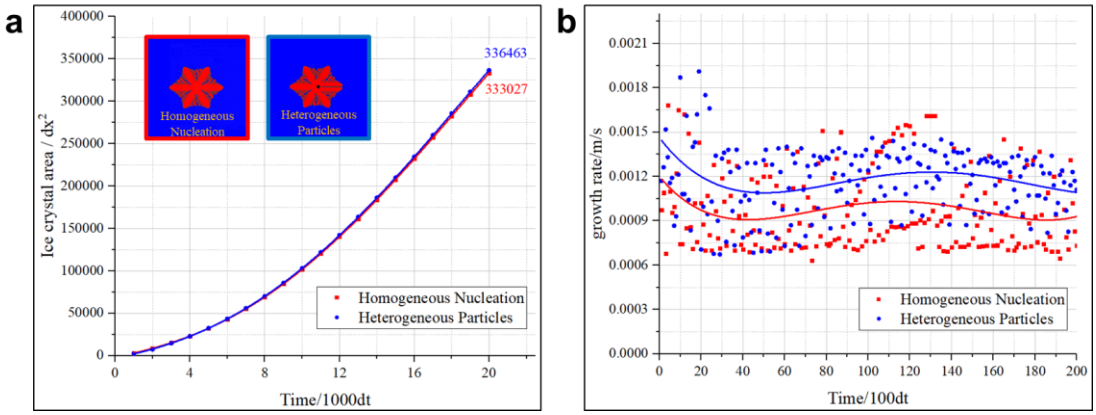

Fig. 13. Analysis of the simulation results of ice crystal area and tip growth rate of ice single-crystal free growth in homogeneous nucleation conditions and under the influence of heterogeneous particles of a: ice crystal area; b: ice crystal growth rate.

Fig. 13 shows the simulation results comparison of single sea ice crystal with different nucleation methods. Although the nucleation stage provides the most fundamental manifestation of the different nucleation methods, it is found do not have a significant influence on the area of free growth of ice single-crystals. Single-crystal free growth, homogeneous nucleation, and heterogeneous nucleation exhibited basically the same change trend for the ice crystal tip growth rate; relatively fast at the beginning and then generally stable. From the numerical analysis, because the thermal properties of heterogeneous particles are better than those of ice crystals, the tip growth rate of ice crystals in the presence of heterogeneous particles is always higher than that in the case of homogeneous nucleation. However, the difference in the area of the ice crystals between the two cases is not large, indicating that the gap between the dendrites of the ice crystals is larger in the case of heterogeneous nucleation, which is consistent with the results of the simulation.

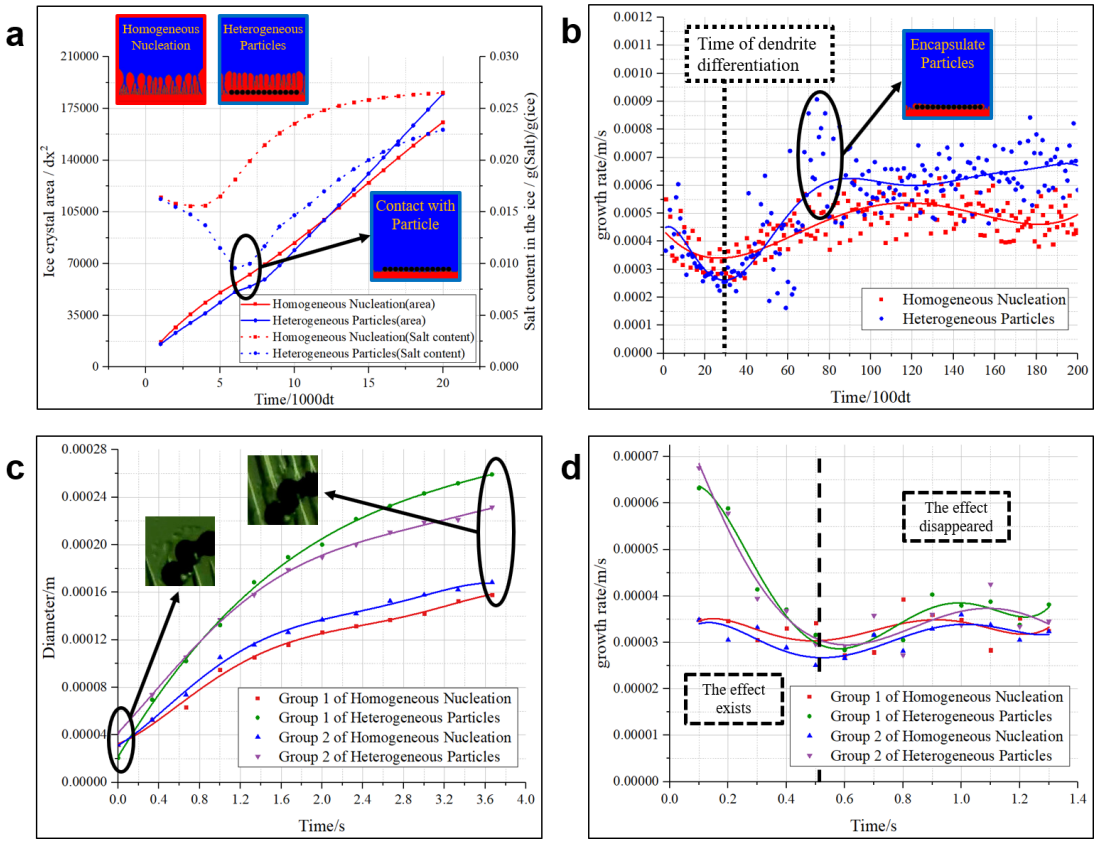

Fig. 14. Simulation and experimental data analyses of the directional competitive growth of sea ice crystals in homogeneous nucleation conditions and under the influence of heterogeneous particles of a: simulated ice crystal area (simulation); b: simulated ice crystal growth rate (simulation); c: experimental dendrite tip diameter (experiment); d: experimental ice crystal growth rate (experiment).

Fig. 14 shows the simulation and experimental results comparison of directional competitive growth of sea ice crystals with or without the impact of homogeneous particles. As is shown in Fig. 14a, in the initial stage of crystallisation, the area of ice crystals under homogeneous nucleation conditions was larger than that under heterogeneous particles. At approximately 7,000 steps, the growth rate of the ice crystal area under the condition of heterogeneous particles was greater than that under the condition of homogeneous nucleation. This is the time at which ice crystals completely enveloped the heterogeneous particles. In the presence of heterogeneous particles, the ice crystal area at 20,000 steps was 10.8% larger than that under homogeneous nucleation conditions. Thus, heterogeneous particles can promote an increase in the ice crystal area to a certain extent. Furthermore, the simulation results show that heterogeneous particles can reduce the salt residue in ice crystals. In the presence of heterogeneous particles, the concentration of ice crystal salt first

decreases and then increases. When the ice crystal contacts with heterogeneous particles, the salt content in the ice reaches the lowest, which is about 48% lower than that in homogeneous nucleation conditions. With the increase of time, the salt content in the ice increases slowly. After the 20000-step iteration, the ice crystal salt content difference between the two cases is about 14.8%.

It is found in Fig. 14b that during the growth period of planar crystals, the growth rates of ice crystals under the two nucleation conditions exhibited downward trends, reaching the lowest at 3,000 steps, and then showed a steady increasing trend. Under the condition of heterogeneous particles, the growth rate of ice crystals in the initial stage of ice crystal growth declined significantly faster than that under homogeneous nucleation conditions. After reaching the lowest speed, the growth rate was also significantly higher than that of ice crystals under homogeneous nucleation conditions. At approximately 5,000 steps, ice crystals started to contact the heterogeneous particles, and the growth rate exceeded and remained greater than that under homogeneous nucleation conditions. At approximately 7,000 steps, the ice crystals enveloped the heterogeneous particles, and the ice crystal growth rate appeared at a maximum. Because the thermal conductivity of heterogeneous particles is better than that of ice crystals, the latent heat released by the growth of ice crystals and bottom heat flux acted on the heterogeneous particles, causing the temperature change of the heterogeneous particles to be greater than that of the ice crystal, and leading to a sharp change in the growth rate of ice crystals.

According to Fig. 14c, in the initial growth stage of ice crystals, the growth rate of dendrite diameter was faster than that of dendrites without heterogeneous particles. because the thermal conductivity of heterogeneous particles is better than that of sea ice crystals, the temperature reduced around the heterogeneous particles. Meanwhile, the existence of heterogeneous particles disturbed the stability of the original free energy, and the interface free energy at the boundary changed suddenly, which promoted crystallisation. After the ice crystals completely encapsulated the heterogeneous particles, the growths of the ice crystals under the two conditions again tended to be the same; as a result, after 2 s, the dendrite growth rates under the two conditions gradually approached on another, and the change rate of diameter with time was basically the same.

As is shown in Fig. 14d, the existence of heterogeneous particles changed the supercooling and free energy distribution at the tip of the ice crystals. With the increase in time, the ice crystals

continued to grow, and the influence of heterogeneous particles gradually decreased. The growth rate of ice crystal tips exhibited a trend of first decreasing and then stabilising. Whereas, in the absence of heterogeneous particles, the growth rate of the ice crystal tip showed a dynamic and stable trend. The values of the ice crystal tip growth rates under the two conditions were similar after stabilisation, indicating that the effect of heterogeneous particles on the growth of ice crystals is mainly concentrated on the ice crystal.

7 Conclusions

This study provides a methodology of numerically simulate sea ice crystallisation which includes the phase change, solute migration, heat transfer and flow, as well as a feasible controlling approach to improve desalination efficiency of sea water frozen crystallisation. Both the single sea ice crystallisation which reflects the suspension freeze crystallisation and the directional competitive sea ice crystallisation which reflects the layer freeze crystallisation were investigated. A four-physical-fields coupling model for sea ice crystallisation was established to conduct the simulation, a high-definition 3D transmission microscope observation experimental system was built up to experimental verify the simulation results. Sea ice crystal morphology, solute diffusion, and heat flux changes during the crystallisation process were investigated. The results show the potential for reducing salt residues and increasing ice crystal production during sea water freezing. Main conclusions are made as follows:

1) The flow of sea water results in the formation of different concentrations and temperature gradients, which promotes the diffusion of discharged salt and the growth of ice crystals, and reduces the probability of dendrite closure.
2) In the directional competitive growth of ice crystals, the salt content in the ice decreased by 17.4% at 0.025 m/s and 21.9% at 0.05 m/s, respectively, although the ice crystal area decreased by 21.8% at 0.025 m/s and 25.3% at 0.05 m/s, respectively.
3) The existence of heterogeneous particles can narrow the brine channel, increase the growth rate and the area of ice crystals.
4) In the directional competitive growth of ice crystals under the condition of heterogeneous particles, the ice crystal area increased by 10.8% and the trapped salt content in the ice crystals decreased by 14.8%.

Appendix A

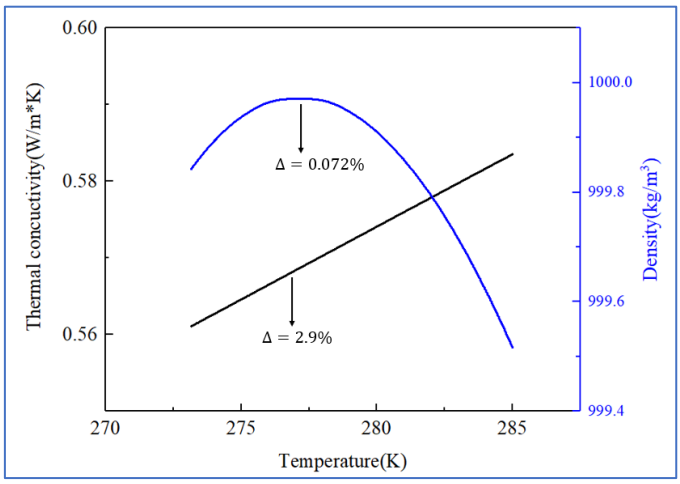

Fig. 15. Thermophysical properties of seawater

Appendix B

The velocity field of single and directional sea ice crystallisation are detailed presented in Fig. 16(a) as the supplementary to Fig. 6 (d1, d2, d3), and Fig. 16(b) as the supplementary to Fig. 7 (d1, d2, d3), respectively.

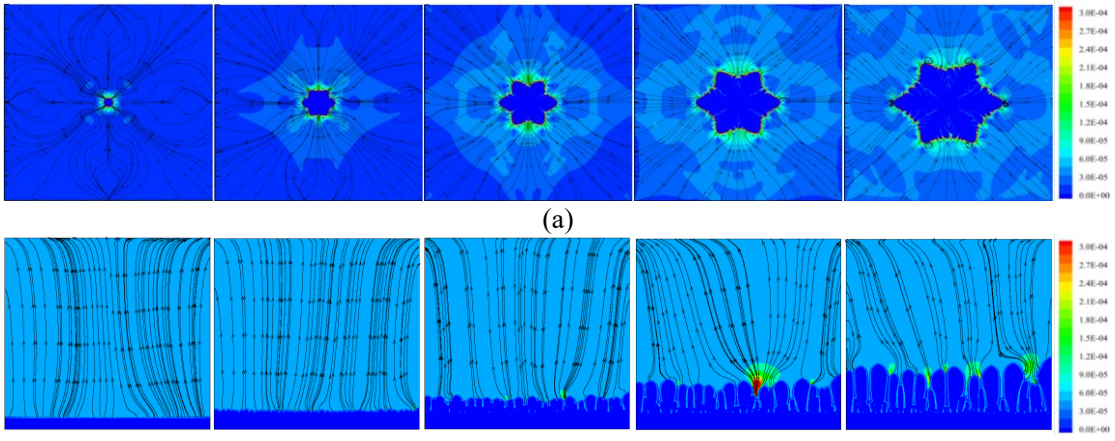

(a)

(b)

Fig. 16. Natural convection velocity field during sea ice crystallisation: (a) single crystallisation; (b) directional crystallisation

Appendix C

The complied C++ program involves coupling solution of multiple field based on different algorithms, and the complication of calculation and data calling results in low simulation efficiency. In order to solve this problem, an adaptive optimization algorithm is proposed. It is worth noting that the numerical values of grids are not always affected by crystallisation during ice crystal growth,

once the grid values remain unchanged, calculation on this part of the grids is jumped. The schematic diagram of optimization algorithm is shown in Fig. 17 and described as follows: firstly, build a 5 × 5 block next to the boundary grid (shown on the bottom left); secondly, randomly select another 5 calculated grids in the block; thirdly, calculate the phase-field parameter and concentration gradient between these grids, once the gradient of phase-field parameter and concentration are less than a small value, it can be considered that the parameters within this block is uniform, therefore the entire block is deemed as a new real-time adaptive upgrading grid.

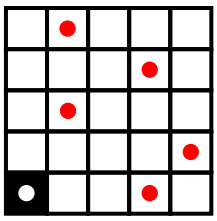

Fig. 17. Schematic diagram of adaptive optimization algorithm

Acknowledgements

The authors acknowledge the support provided by the National Natural Science Foundation of China (51706214), the demonstration and guidance project of science and technology benefiting people in Qingdao (21-1-4-sf-15-nsh) and Natural Science Foundation of Shandong (ZR2020me186).

References:

[1] E. Chafik, Design of plants for solar desalination using the multi-stag heating/humidifying technique, DESALINATION, 168 (2004) 55-71.
[2] C. Qi, H. Lv, H. Feng, Q. Lv, Y. Xing, Performance and economic analysis of the distilled seawater desalination process using low-temperature waste hot water, APPL. THERM. ENG., 122 (2017) 712-722.
[3] H. Yang, Z. Zhan, Y. Yao, Z. Sun, Influence of gravity-induced brine drainage on seawater ice desalination, DESALINATION, 407 (2017) 33-40.
[4] B. Kalista, H. Shin, J. Cho, A. Jang, Current development and future prospect review of freeze desalination, DESALINATION, 447 (2018) 167-181.
[5] P. Gao, Z. Guo, D. Zhang, X. Zhou, G. Zhou, Performance analysis of evaporation-freezing desalination system by humidity differences, DESALINATION, 347 (2014) 215-223.
[6] M.S. Rahman, M. Ahmed, X.D. Chen, Freezing melting process and desalination: review of present status and future prospects, International Journal of Nuclear Desalination, 2 (2007) 253-264.
[7] B. Kalista, H. Shin, J. Cho, A. Jang, Current development and future prospect review of freeze desalination, DESALINATION, 447 (2018) 167-181.
[8] C. Xie, L. Zhang, Y. Liu, Q. Lv, G. Ruan, S.S. Hosseini, A direct contact type ice generator for seawater freezing desalination using LNG cold energy, DESALINATION, 435 (2018) 293-300.
[9] H. Yuan, P. Sun, J. Zhang, K. Sun, N. Mei, P. Zhou, Theoretical and experimental investigation of an absorption refrigeration and pre-desalination system for marine engine exhaust gas heat recovery, APPL. THERM. ENG., 150 (2019) 224-236.
[10] M. Mahdavi, A.H. Mahvi, S. Nasseri, M. Yunesian, Application of Freezing to the Desalination of Saline Water, ARAB. J. SCI. ENG., 36 (2011) 1171-1177.
[11] D.M. Cole, L.H. Shapiro, Observations of brine drainage networks and microstructure of first-year sea ice, Journal of Geophysical Research: Oceans, 103 (1998) 21739-21750.
[12] C. Petrich, H. Eicken, Growth, Structure and Properties of Sea Ice, 2009, pp.23-77.
[13] J. Chang, J. Zuo, K. Lu, T. Chung, Freeze desalination of seawater using LNG cold energy, WATER RES., 102 (2016) 282-293.

[14] L. Xie, J. Ma, F. Cheng, P. Li, J. Liu, W. Chen, S. Wang, Study on sea ice desalination technology, DESALINATION, 245 (2009) 146-154.
[15] M. Wakisaka, Y. Shirai, S. Sakashita, Ice crystallization in a pilot-scale freeze wastewater treatment system, Chemical Engineering and Processing: Process Intensification, 40 (2001) 201-208.
[16] W. Gao, D.W. Smith, D.C. Sego, Treatment of pulp mill and oil sands industrial wastewaters by the partial spray freezing process, WATER RES., 38 (2004) 579-584.
[17] W.T. Hung, W.H. Feng, I.H. Tsai, D.J. Lee, S.G. Hong, Uni-directional freezing of waste activated sludges: Vertical freezing versus radial freezing, WATER RES., 31 (1997) 2219-2228.
[18] G. Gay, O. Lorain, A. Azouni, Y. Aurelle, Wastewater treatment by radial freezing with stirring effects, WATER RES., 37 (2003) 2520-2524.
[19] G.M. Westhoff, H.J.M. Kramer, Scale-up of suspension crystallisers using a predictive model framework, CHEM. ENG. SCI., 77 (2012) 26-34.
[20] K. Watanabe, Y. Muto, M. Mizoguchi, Water and Solute Distributions near an Ice Lens in a Glass-Powder Medium Saturated with Sodium Chloride Solution under Unidirectional Freezing, CRYST. GROWTH DES., 1 (2001) 207-211.
[21] J.S. Langer, Models of pattern formation in first-order phase transitions, Directions in Condensed Matter Physics, (1986) 165-186.
[22] P.C. Hohenberg, A.P. Krekhov, An introduction to the Ginzburg–Landau theory of phase transitions and nonequilibrium patterns, Physics Reports, 572 (2015) 1-42.
[23] G. Da Prato, V.D. Rădulescu, Special issue on stochastic PDEs in fluid dynamics, particle physics and statistical mechanics, J. MATH. ANAL. APPL., 384 (2011) 1.
[24] C. Beckermann, H.J. Diepers, I. Steinbach, A. Karma, X. Tong, Modeling Melt Convection in Phase-Field Simulations of Solidification, J. COMPUT. PHYS., 154 (1999) 468-496.
[25] X. Tong, C. Beckermann, A. Karma, Q. Li, Phase-field simulations of dendritic crystal growth in a forced flow, PHYS. REV. E, 63 (2001).
[26] V. Berti, M. Fabrizio, D. Grandi, A phase field model for brine channels in sea ice, Physica B: Condensed Matter, 425 (2013) 100-104.
[27] R.G.M. van der Sman, Phase field simulations of ice crystal growth in sugar solutions, INT. J. HEAT MASS TRAN., 95 (2016) 153-161.
[28] D.F. HAN, Y.K. WANG, L. Ju, Q. Wang, Phase field simulation of ice crystal growth in seawater freezing process, Journal of Harbin Engineering University, 41 (2020) 1-8.
[29] H. Yuan, K. Sun, K. Wang, J. Zhang, Z. Zhang, L. Zhang, S. Li, Y. Li, Ice crystal growth in the freezing desalination process of binary water-NaCl system, DESALINATION, 496 (2020) 114737.
[30] S.G. Kim, W.T. Kim, T. Suzuki, Phase-field model for binary alloys, PHYS. REV. E, 60 (1999) 7186-7197.
[31] R.G.M. van der Sman, Multiscale simulations of directional ice crystal growth in sugar solutions, Food Structure, 30 (2021) 100214.
[32] E. Liotti, A. Lui, S. Kumar, Z. Guo, C. Bi, T. Connolley, P.S. Grant, The spatial and temporal distribution of dendrite fragmentation in solidifying Al-Cu alloys under different conditions, ACTA MATER., 121 (2016) 384-395.
[33] T. Basak, R. Anandalakshmi, P. Kumar, S. Roy, Entropy generation vs energy flow due to natural convection in a trapezoidal cavity with isothermal and non-isothermal hot bottom wall, ENERGY, 37 (2012) 514-532.
[34] A. Rajantie, Vortices and the Ginzburg–Landau phase transition, Physica B: Condensed Matter, 255 (1998) 108-115.
[35] J.A. Warren, W.J. Boettinger, Prediction of dendritic growth and microsegregation patterns in a binary alloy using the phase-field method, Acta Metallurgica et Materialia, 43 (1995) 689-703.
[36] S.G. Kim, W.T. Kim, T. Suzuki, Interfacial compositions of solid and liquid in a phase-field model with finite interface thickness for isothermal solidification in binary alloys, PHYS. REV. E, 58 (1998) 3316-3323.
[37] G.B. McFadden, A.A. Wheeler, R.J. Braun, S.R. Coriell, R.F. Sekerka, Phase-field models for anisotropic interfaces, PHYS. REV. E, 48 (1993) 2016-2024.
[38] J. van Mill, A. Ran, On a generalization of Lyapounov's theorem, Indagationes Mathematicae, 7 (1996) 227-242.
[39] N. Moelans, B. Blanpain, P. Wollants, An introduction to phase-field modeling of microstructure evolution, CALPHAD, 32 (2008) 268-294.
[40] A.A. Wheeler, W.J. Boettinger, G.B. McFadden, Phase-field model for isothermal phase transitions in binary alloys, PHYS. REV. A, 45 (1992) 7424-7439.
[41] A.A. Wheeler, B.T. Murray, R.J. Schaefer, Computation of dendrites using a phase field model, Physica D: Nonlinear Phenomena, 66 (1993) 243-262.

[42] S. Wang, R.F. Sekerka, Algorithms for Phase Field Computation of the Dendritic Operating State at Large Supercoolings, J. COMPUT. PHYS., 127 (1996) 110-117.
[43] Da Zhang, Sufen Li, Si jiao, Yan Shang, Ming Dong. Relative permeability of three immiscible fluids in random porous media determined by the lattice Boltzmann method[J]. International Journal of Heat and Mass Transfer 134 (2019) 311–320.
[44] Da Zhang, Sufen Li, Weiyu Ren, Yan Li, Ning Mei. Co-existing boiling and condensation phase changes of a multicomponent fluid in a confined micro-space analysed by a modified LBM[J]. International Journal of Thermal Sciences 170 (2021) 107147.
[45] S. Chen, H. Chen, D. Martnez, W. Matthaeus, Lattice Boltzmann model for simulation of magnetohydrodynamics, PHYS. REV. LETT., 67 (1991) 3776-3779.
[46] W. Miller, S. Succi, D. Mansutti, Lattice Boltzmann Model for Anisotropic Liquid-Solid Phase Transition, PHYS. REV. LETT., 86 (2001) 3578-3581.
[47] S. Ding, X. Huang, Q. Yin, Y. Dong, Y. Bai, T. Wang, H. Hao, Heat transfer and its effect on growth behaviors of crystal layers during static layer melt crystallization, CHEM. ENG. SCI., 233 (2021) 116390.
[48] Milan Chandra Barma, Zhengbiao Peng, Behdad Moghtaderi, Elham Doroodchi. Freeze desalination of drops of saline solutions. Desalination 517 (2021) 115265.
[49] Michael F. Butler. Instability Formation and Directional Dendritic Growth of Ice Studied by Optical Interferometry. Crystal Growth & Design, Vol. 1, No. 3, 2001.
[50] J. Vymazal, T. Březinová, Accumulation of heavy metals in aboveground biomass of Phragmites australis in horizontal flow constructed wetlands for wastewater treatment: A review, CHEM. ENG. J., 290 (2016) 232-242.
[51] J.E. Castillo, Y. Huang, Z. Pan, J.A. Weibel, Quantifying the Pathways of Latent Heat Dissipation during Droplet Freezing on Cooled Substrates, INT. J. HEAT MASS TRAN., 164 (2021) 120608.
[52] S. Liu, L. Hao, Z. Rao, X. Zhang, Experimental study on crystallization process and prediction for the latent heat of ice slurry generation based sodium chloride solution, APPL. ENERG., 185 (2017) 1948-1953.
[53] M. El-Shahed, A. Salem, Decay of vortex velocity and diffusion of temperature for fractional viscoelastic fluid through a porous medium, INT. COMMUN. HEAT MASS, 33 (2006) 240-248.
[54] S. Ogawa, S. Osanai, Solute- and concentration-dependent heterogeneous ice nucleation behaviors in AgI composite water droplets, CHEM. PHYS. LETT., 754 (2020) 137775.
[55] M. Tomellini, S. Politi, Kinetics of phase transformations with heterogeneous correlated-nucleation, Physica A: Statistical Mechanics and its Applications, 513 (2019) 175-188.
[56] T. Fujinaga, Y. Shibuta, Molecular dynamics simulation of athermal heterogeneous nucleation of solidification, COMP. MATER. SCI., 164 (2019) 74-81.

Author contributions

J. S. completed the preparation of the simulation program, designed and conducted experiments, completed the subsequent data analysis and wrote manuscript. H. Y. conceived and designed this project, provided thought guidance, wrote part of the manuscript and revised manuscript. J. Z. and D. Z. assisted in data analysis and summary. P. Z., Y. L. and N. M. provided consultant. K. W. assisted in the experimental results analysis.